MADRID
inter.noise 2019
June 16 - 19
NOISE CONTROL FOR A BETTER ENVIRONMENT

Characteristics of Sound Radiated due to Flow Around a Rotationally Oscillating Cylinder

Ganta, Naveen[1]; Mahato, Bikash[2]; Bhumkar, Yogesh G.[3]
Scientific Computing Laboratory, School of Mechanical Sciences, Indian Institute of Technology Bhubaneswar, Odisha, India-752050

ABSTRACT

Direct simulations have been performed to study the sound field radiated due to two-dimensional unsteady flow past a circular cylinder performing rotary oscillations. Effects of forcing frequency and amplitude of oscillation on the radiated sound fields have been analyzed using higher resolution dispersion relation preserving (DRP) schemes. The computations are performed on a highly refined structured grid at a Reynolds number $Re_\infty = 150$ and Mach number $M_\infty = 0.2$. The phenomena of synchronization and non-synchronization of shedding patterns are observed. In the synchronous region, both fluctuating loads acting on the cylinder and their corresponding sound fields are completely governed by forcing frequency-ratio. In the non-synchronous region, the generated sound fields exhibit modulation phenomena such that the signal is governed by forcing frequency-ratio as well as frequency-ratio corresponding to shedding frequency of a stationary cylinder for the same free-stream conditions. Directivity patterns based on root mean square (RMS) values of disturbance pressure fields are obtained and they are found to be dipolar nature dominated by lift dipole. Various dominant modes related to sound field are obtained using the analysis of proper orthogonal decomposition (POD). These POD modes have further helped us to understand the generated sound fields in a better manner.

Keywords: Bluff body flows, Rotary oscillations, Aerodynamic noise
I-INCE Classification of Subject Number: 20

1. INTRODUCTION

Flow past bluff bodies has been the topic of great interest for many researchers and engineers. It has wide range of engineering applications such as bridge pillars, wind turbines, skyscrapers and landing gear of aeroplane. Smooth functioning of these

[1]ng13@iitbbs.ac.in
[2]bm18@iitbbs.ac.in
[3]bhumkar@iitbbs.ac.in

applications demands proper understanding of not only the flow features, but also the aerodynamic noise features. During the process of vortex shedding for laminar flow past a circular cylinder, acoustic pressure pulses (aerodynamic noise) are generated primarily due to fluctuations in aerodynamic forces acting on cylinder surface, and the resultant acoustic field is known to be of dipolar nature [1, 2, 3, 4].

Computational Aero-Acoustics (CAA) is a branch that involves the study of aerodynamic noise using numerical schemes. Researchers have performed Direct Numerical Simulations (*DNS*) to obtain sound generated for laminar flow past stationary bluff bodies such as circular, square and rectangular cylinders [5, 6, 7, 8]. However, very few computational studies have addressed aerodynamic noise generated during flow past oscillating bluff bodies based on *DNS* approach [9, 10, 11].

In the present study, two-dimensional, unsteady laminar flow past a circular cylinder performing rotary oscillations is conducted based on *DNS* approach in order to accurately resolve both flow and aerodynamic noise features. Various dominant modes of the resultant disturbance pressure field are analyzed using proper orthogonal decomposition analysis [12, 13].

2. METHODOLOGY

2.2.1. Problem Description

The schematic of a circular cylinder with diameter D=1 m performing periodic rotary oscillations is shown in Fig. 1. The Reynolds number and Mach number are defined as $Re_\infty = (\rho_\infty U_\infty D)/\mu_\infty$ and $M_\infty = U_\infty/a_\infty$, respectively. Here, ρ_∞, U_∞, μ_∞ and a_∞ account for free-stream parameters such as density, velocity, viscosity and speed of sound associated with free-stream absolute temperature T_∞, respectively. The Strouhal number of a stationary cylinder with vortex shedding frequency f_o is given as $S_o = f_o D/U_\infty$.

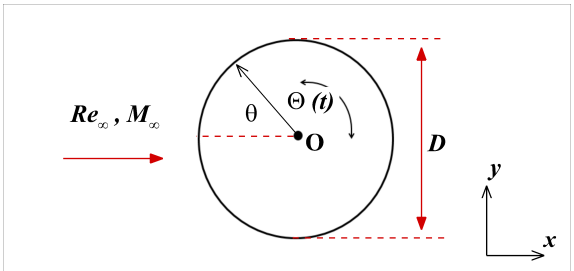

Figure 1: Flow over a cylinder performing rotary oscillations.

The instantaneous rotation rate $\Omega(t)$ of an oscillating cylinder is given by

$$\Omega(t) = \Omega_1 sin(2\pi S_f t) \tag{1}$$

where, $\Omega_1 = 2\pi f_f \alpha_o$ denotes maximum rotation rate with maximum angular displacement as α_o and forcing frequency as f_f. Strouhal number based on forcing frequency f_f is given as $S_f = (f_f D)/U_\infty$. Tangential velocity on the cylinder is prescribed using the non-dimensional parameters such as frequency-ratio $f_r = f_f/f_o$ and forcing amplitude $A = \Omega_1 D/(2U_\infty)$ [11]. Free stream flow is prescribed along the positive $x-$ direction with $Re_\infty = 150$, $M_\infty = 0.2$, $\rho_\infty = 1.12 kg/m^3$, and $T_\infty = 288K$.

2.2.2. Grid details and Numerical procedure

Circular cylinder is placed at the center of an $O-$grid topology with outer boundary set at a radial distance $r = 1500D$ measured from origin O. Let θ be the angle made by a radial line with the negative $x-$axis as shown in Fig. 1. In order to accurately resolve aeroacoustic noise, highly refined structured grid has been adopted near the cylinder surface and this zone is termed as sound zone ($0.5D \leq r \leq 100D$). Coarse grid has been chosen in the far-field and this zone is known as buffer zone ($100D < r \leq 1500D$). The schematic of grid structure has been reported in [11] and is not shown here to avoid repetition. Convergence limits of flow parameters are dependent on choice of grid resolution and hence, grid convergence study has also been conducted for flow past a stationary circular cylinder [11]. Based on grid convergence study, adequate number of grid points in the azimuthal direction (θ) and radial direction (r) are considered as 501 and 900, respectively.

Two-dimensional, unsteady compressible fluid flow equations in the conservative form are considered along with the equation of state. [14] The equations are non-dimensionalized using free-stream parameters. The lengths x, y and r are scaled by D. $x-$ and $y-$ direction velocity components (u & v) are normalized using U_∞. Density (ρ), pressure (p), temperature (T) and time (t) are non-dimensionalized using ρ_∞, $\rho_\infty U_\infty^2$, T_∞ and D/U_∞, respectively. From here, non-dimensional parameters have been denoted as x, y, r, t, u, v, p, ρ and T. As our computations are based on finite difference compact schemes, the governing equations are transformed from physical space to computational space using the method of grid transformation [14].

Non-linear convective terms and grid derivative terms are discretized using high resolution Optimized Coupled Compact Difference ($OCCD$) scheme [15, 16]. Optimized five stage Runge-Kutta ($ORK5$) scheme has been chosen for time integration [17]. Viscous derivative terms are discretized using traditional central difference schemes of second order accurate.

3. RESULTS AND DISCUSSION

Computations are performed for sufficiently long duration and periodic shedding of vortices are observed. Time averaging procedure has been conducted for more than 10 shedding cycles. Thiria et al. [18] has performed water tunnel experiments for flow over rotationally oscillating cylinder at $Re_\infty = 150$ and they found that the non-dimensional shedding frequency of flow past stationary circular cylinder at $f_o = 0.1633$. In order to validate our results with experimental results of Thiria et al. [18], the frequency-ratio $f_r = f_f/f_o$ is evaluated based on $f_o = 0.1633$. Strouhal number of stationary cylinder obtained from the present computations is found to be 0.182 and the corresponding frequency-ratio (is denoted as f_s) is given as $f_r = f_s = 0.182/0.1633 \approx 1.11$. Hence, $f_r = 1.11$ represents the frequency-ratio corresponding to natural shedding frequency of flow past a stationary cylinder. A detailed Validation and verification studies of flow as well as sound field parameters are reported in our previous study [11] and are not shown here to avoid repetition. Present DNS study is carried out on a two-dimensional domain for various values of forcing frequency-ratio ($0.0 \leq f_r \leq 2.0$) for an oscillating amplitude $A = 0.2$. Mean and fluctuating parameters are evaluated and are discussed.

Time averaged lift (C_{Lf}) and drag (C_{Df}) coefficients are evaluated for all values of f_r considered in the present study. The value of C_{Lf} is found to be zero for all forcing

conditions. Drag coefficient of flow over a stationary cylinder at $Re = 150$ is denoted as C_{Do}. Variation of normalized drag coefficient (C_{Df}/C_{Do}) with f_r is shown in Fig. 2 (a). As f_r increases, normalized drag coefficient has remained almost constant and is equal to that of a stationary cylinder case ($C_{Df}/C_{Do} = 1.0$) until $f_r = 0.5$ and then it drops at $f_r = 0.9$. But in the range $0.9 \leq f_r \leq 1.11$, the value of C_{Df}/C_{Do} is increased gradually, which is due to the establishment of effective synchronization between the incoming flow and cylinder oscillation. In rest of the f_r range, C_{Df}/C_{Do} value is almost same as that observed for a stationary cylinder case. At $f_r = 0.9$, the drag value ($C_{Df}/C_{Do} = 0.92$) is relatively lower as compared to flow past a cylinder without oscillation ($C_{Df}/C_{Do} = 1.0$).

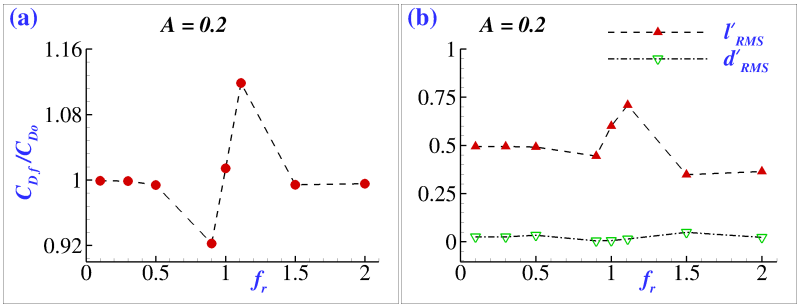

Figure 2: (a) Variation of normalized drag coefficient C_{Df}/C_{Do} with frequency-ratio. (b) Variation of RMS values of l' and d' with f_r.

Process of vortex shedding triggers fluctuations in aerodynamic forces which are found responsible for generation of aerodynamic noise for flow past a cylinder at low Mach numbers [1, 5]. Relative magnitudes of lift and drag fluctuations and the phase difference between them decide the nature and strength of net radiated sound fields. Hence, fluctuations in lift (l') and drag (d') coefficients have been evaluated. Figure 2 (b) represents the variation of root mean square values RMS of lift and drag coefficients (l'_{RMS} & d'_{RMS}) with frequency-ratio. The magnitudes of d'_{RMS} are much lower as compared to the values of l'_{RMS}. The RMS values of d' are almost negligible as compared to the values of l'_{RMS}. Variation of l'_{RMS} with f_r shows a similar trend as observed for a normalized drag coefficient.

Figure 3 shows the variation of fluctuations in lift and drag coefficients (l' & d') with time for different values of f_r considered at $A = 0.2$. The phenomenon of modulation has been observed for both time varying lift and drag fluctuations in the range $f_r < 0.9$ & $f_r > 1.11$. This region belongs to non-synchronous zone where the vortex shedding patterns are not completely governed by forcing frequency alone. In the range $0.9 \leq f_r \leq 1.11$, no modulation phenomenon has been found and also the shedding patterns occur at forcing frequency alone. Similar features of synchronous and non-synchronous zones of flow past a rotationally oscillating cylinder has already been reported in the literature. It is also observed that for a given f_r value, the magnitudes of fluctuations in lift coefficient are much higher as compared to that of drag fluctuations. Further, amplitude of time varying l' is relatively higher for $f_r = 1.0$ & 1.11 cases.

Fast Fourier transform (FFT) of time varying l' has been evaluated for different values of f_r and is shown in Fig. 4. In Fig. 4 (a), for a given forcing condition,the peaks of l' are identified at forcing frequency-ratio $f_{r1} = f_r$ and at the frequency-ratio $f_{r1} = f_s = 1.11$ which corresponds to the natural shedding frequency observed for a stationary cylinder case. Due to the existence of these two frequencies ($f_{r1} = f_r$ & f_s), modulation phenomena

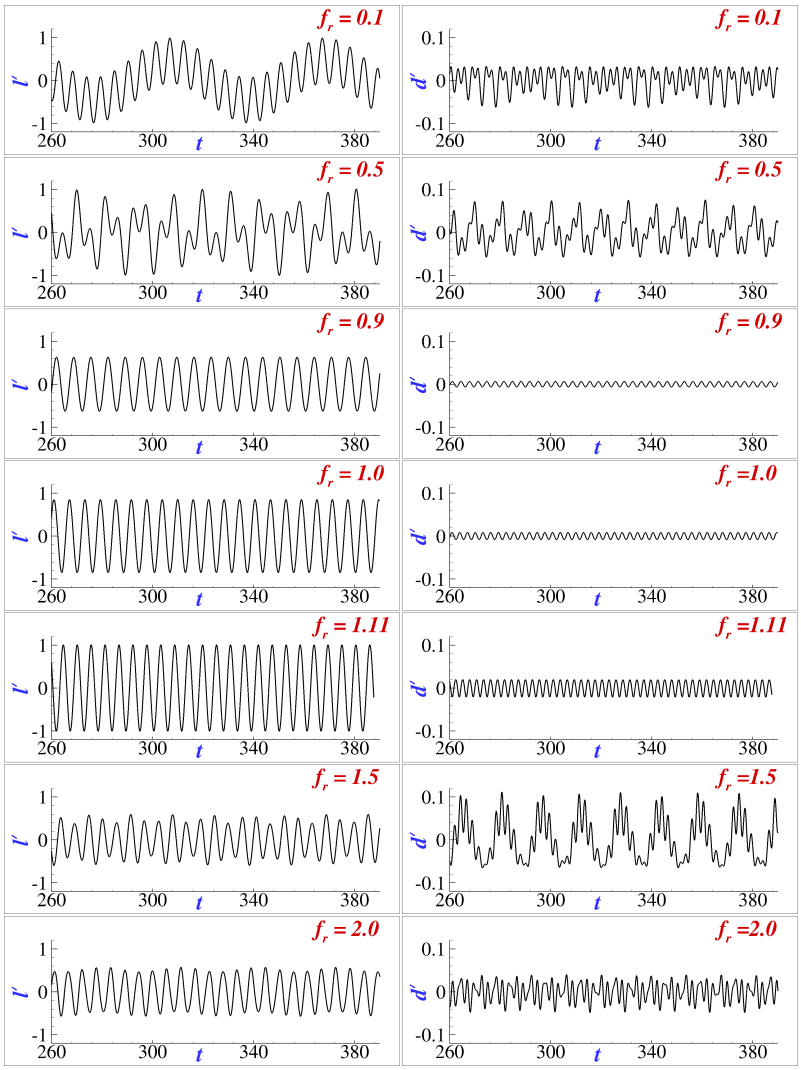

Figure 3: Time variation of fluctuations in lift and drag coefficients are represented here for different values of f_r at $A = 0.2$.

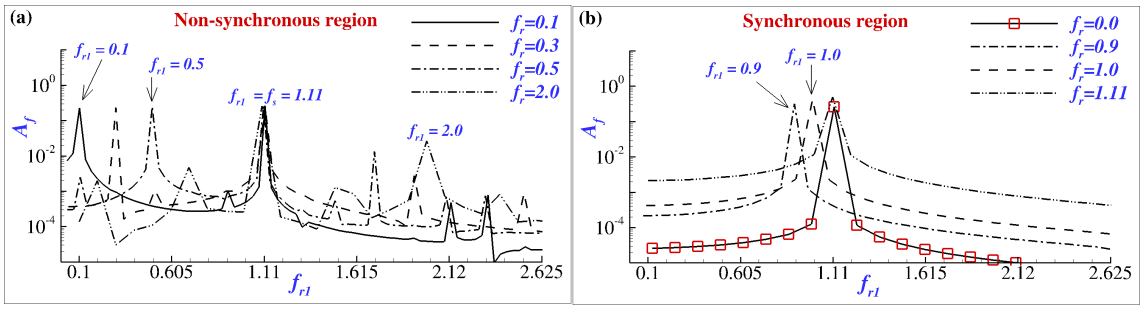

Figure 4: Fast Fourier transform of $l'(t)$ has been shown here for various values of f_r.

has been observed. This frequency spectrum has clearly confirmed that the shedding patterns observed in the range $f_r < 0.9$ & $f_r > 1.11$ are not just governed by forcing frequency-ratio f_r, but also affected by natural shedding frequency of stationary cylinder f_s. In Fig. 4 (b), FFT of l' variation has been displayed for the range $0.9 \leq f_r \leq 1.11$,

where a single peak has been identified at forcing frequency-ratio $f_{r1} = f_r$. The case with $f_r = 0.0$ accounts for flow past a stationary cylinder and the peak has been identified at $f_{r1} = f_s = 1.11$. It is clear that the vortex shedding patterns in the range $0.9 \leq f_r \leq 1.11$ are completely governed by forcing frequency f_r for $A = 0.2$. Therefore, this zone is confirmed as synchronous zone.

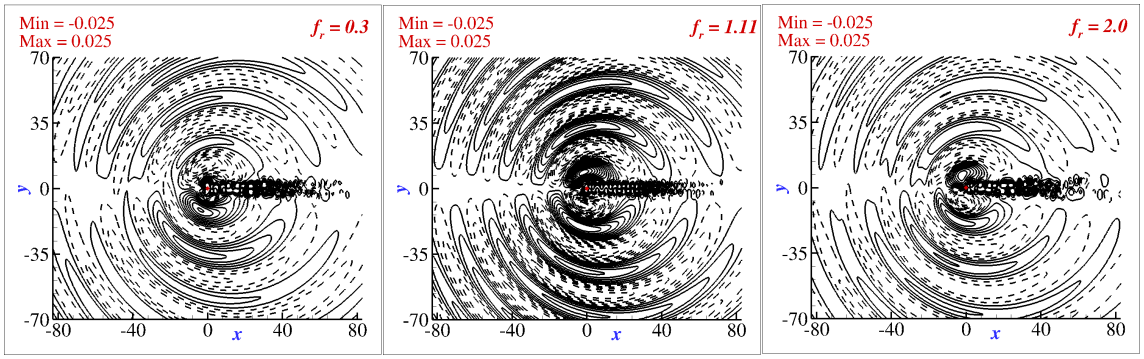

Figure 5: Disturbance pressure fields p' are shown here for three different values of f_r at time $t = 271$.

Figure 5 shows the disturbance pressure fields (p') obtained for indicated values of f_r at a non-dimensional time $t = 271$. Solid and dashed lines represent positive and negative values of p', respectively. In other words, regions of compression and rarefaction are represented by solid and dashed lines, respectively. Contour levels vary from -0.025 to 0.025 with 30 equispaced levels. Disturbance pressure pulses radiate from the cylinder surface and then they propagate away from the cylinder. Alternate shedding of vortices from top and bottom surfaces of cylinder has triggered the generation of disturbance pressure pulses. Further, these disturbance pressure pulses are found to propagate almost in the normal direction of the free-stream direction. This is due to higher amplitudes of lift fluctuations as compared to drag fluctuations. Hence, the net radiated sound must be dominated by lift dipole as proven later using directivity patterns. The case with $f_r = 1.11$ shows relatively more intensity than other f_r cases. This is justified as the magnitude of fluctuations in lift forces is higher in the case of $f_r = 1.11$ as compared to other f_r cases.

Figure 6 (a) shows the variation of p' with time at a location $(r,\ \theta) = (75,\ 90^o)$ for the cases with $f_r = 0.5$ and $f_r = 1.11$. Modulation in p' has been observed for $f_r = 0.5$ case, as the chosen value of f_r is in non-synchronous region. However no such modulation has been observed for $f_r = 1.11$ case which lies in synchronous region. Figure 6 (b) represents FFTs of time varying disturbance pressure profiles extracted for these two f_r values at $(r,\ \theta) = (75,\ 90^o)$. For $f_r = 1.11$ case (in synchronization region), the Fourier peak is observed only at forcing frequency-ratio $f_{r1} = f_r = 1.11$, while for $f_r = 0.5$ case (in non-synchronization region), the Fourier peaks are identified at both forcing frequency-ratio ($f_{r1} = f_r = 0.5$) as well as at the frequency-ratio which corresponds to natural shedding frequency of a stationary cylinder ($f_{r1} = f_s = 1.11$).

According to Curle's analogy, the acoustic pressure p' in the far-field decays as $p' \propto r^{-0.5}$ [1,5]. Fourier amplitudes of $p'(t)$ corresponding to the dominant frequency peak are extracted along the radial distance at an azimuthal angle $\theta = 90^o$. Figure 7 (a) displays the variation in Fourier amplitude of disturbance pressure $A(p')$ with radial distance for indicated values of f_r. Decay of $A(p')$ with radial distance r obeys the theoretical decay rate $p' \propto r^{-0.5}$ over a long distance $r \leq 100$. The amplitudes of p' are much higher for

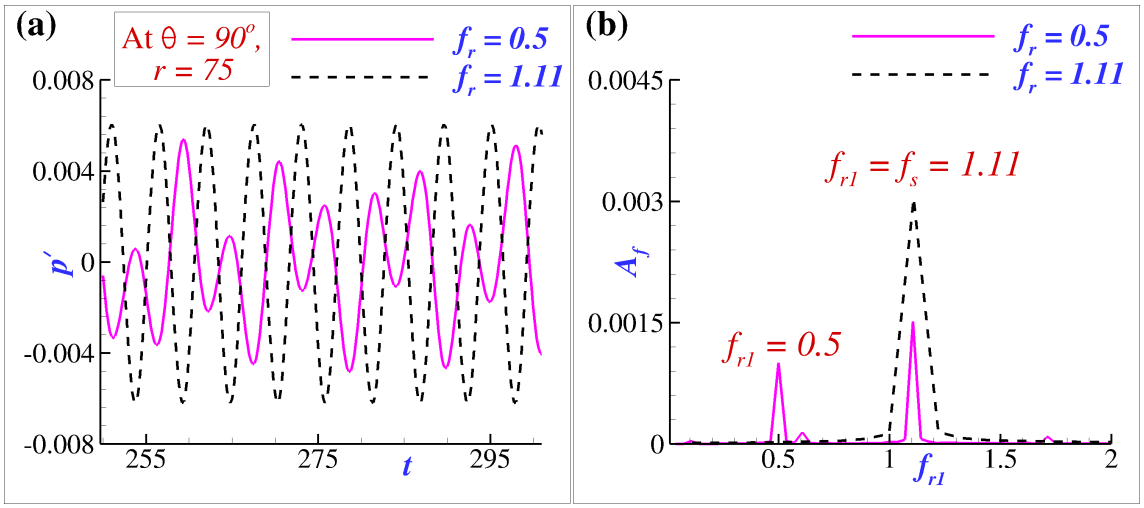

Figure 6: (a) Variation of disturbance pressure with time at $(r,\ \theta) = (75,\ 90^o)$ is shown here for indicated values of f_r. (b) FFTs of these time varying disturbance pressure profiles are displayed.

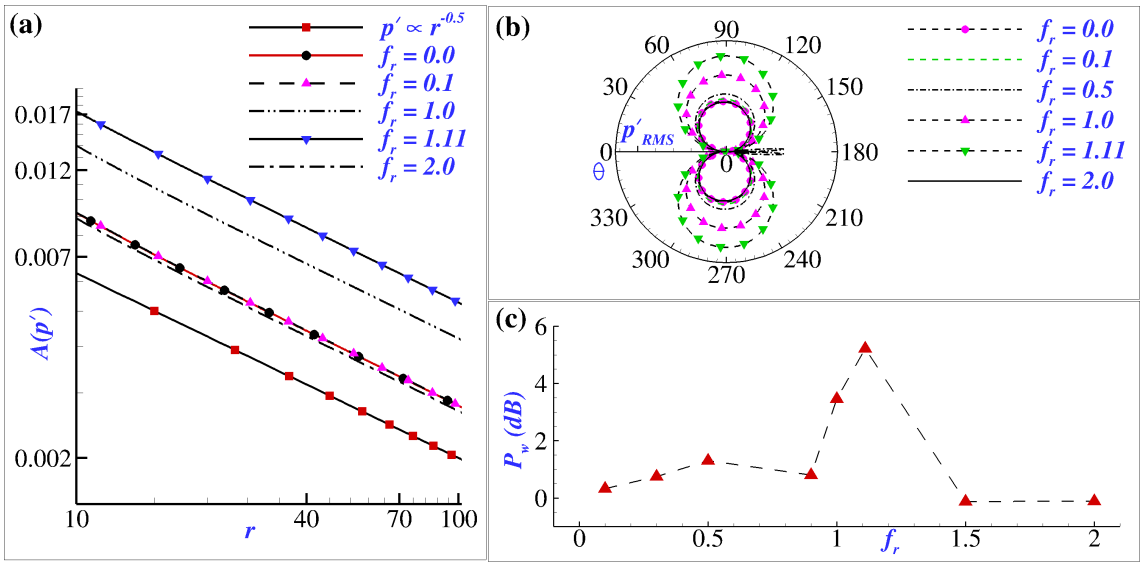

Figure 7: (a) Decay of Fourier amplitudes (corresponding to the dominant frequency peak) of disturbance pressure $A(p')$ with radial distance at $\theta = 90^o$ has been shown. Reference theoretical decay rate is denoted as $p' \propto r^{-0.5}$ [1, 5]. (b) Directivity patterns based on RMS values of p' evaluated at $r = 75$ are shown for indicated values of f_r. (c) Variation of radiated sound power P_w (evaluated at $r = 75$ based on p'_{RMS}) with f_r has been displayed.

$f_r = 1.0$ & $f_r = 1.11$ cases as compared to other values of f_r. In the non-synchronous region ($f_r > 1.11$ & $f_r < 0.9$), the magnitude levels of $A(p')$ are almost same and equal to that of a stationary cylinder case represented as $f_r = 0.0$, although the modulation patterns observed for l' and d' are significantly different.

Figure 7 (b) shows the directivity patterns based on *RMS* values of p' obtained at $r = 75$ for various values of f_r. Similar to the stationary cylinder case (indicated as

$f_r = 0.0$), directivity patterns of net radiated sound fields of an oscillating cylinder are also dominated by lift dipole as magnitudes of lift fluctuations are much higher as compared to magnitudes of drag fluctuations. Sound field strength is higher for $f_r = 1.0$ & $f_r = 1.11$ cases as compared to other values of f_r. Net radiated acoustic power (P_w in dB) has been evaluated using the RMS values of p' obtained at $r = 75$ for different values of f_r as shown in Fig. 7 (c). There is no much significant variation of P_w in the non-synchronous region and relatively higher acoustic power radiation is observed at $f_r = 1.0$ & $f_r = 1.11$. These patterns are similar to the patterns shown in Fig. 7 (b).

Next, the analysis of Proper Orthogonal Decomposition (POD) based on the method of snapshots has been performed for disturbance pressure fields to obtain dominant POD modes and the procedure is similar to the previous studies [11, 15, 12, 19, 13, 20]. The disturbance pressure field can be represented as,

$$p'(x, y, t) = \sum_{n=1}^{N} a_n(t)\, \phi_n(x, y) \tag{2}$$

where, N is number of solution files (snapshots) as considered in the method of snapshots. Time dependent POD amplitudes and eigenfunctions are denoted by $a_n(t)$ and $\phi_n(x, y)$, respectively. The POD analysis also quantify importance of various modes based on respective energy content as given by eigenvalues (λ_k) of a covariance matrix $R_{i,j}$ formed by p'.

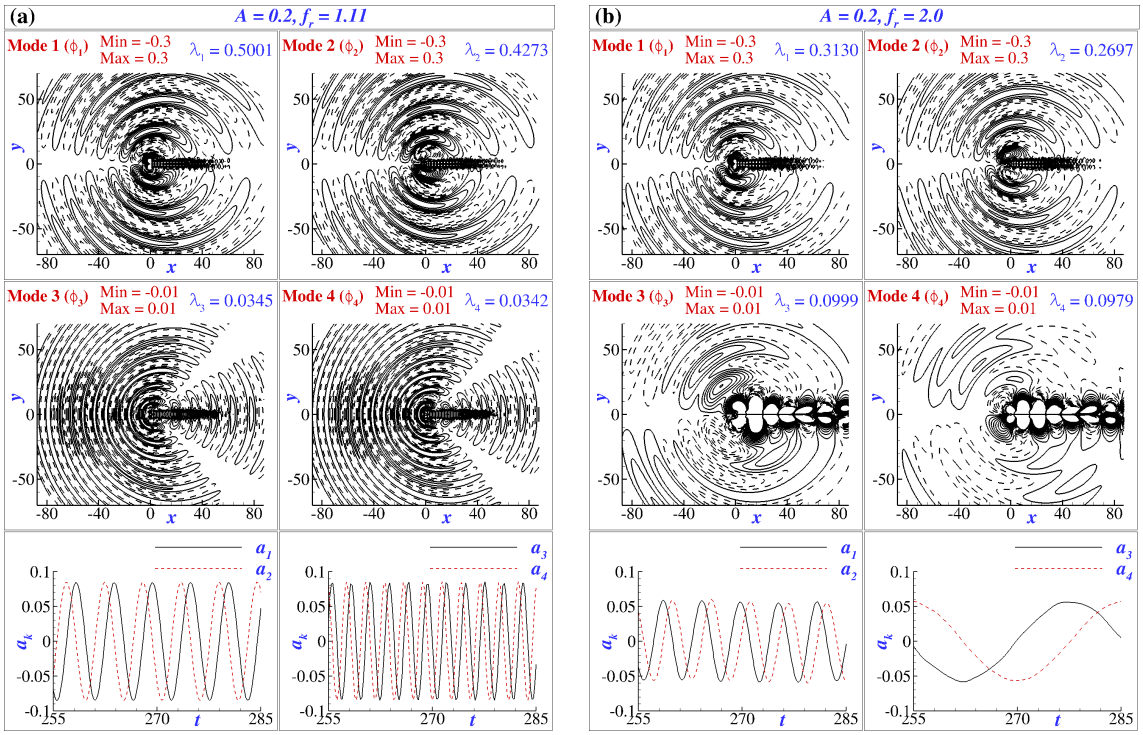

Figure 8: First four dominant POD modes ($\phi_n(x, y)$) and corresponding time varying POD amplitudes ($a_n(t)$) are obtained for disturbance pressure fields at A = 0.2. Frames (a) and (b) display the POD results for the cases with $f_r = 1.11$ and $f_r = 2.0$, respectively. Positive and negative values of POD modes are represented by solid and dashed lines, respectively.

Figure 8 shows the first four dominant *POD* modes $\phi_n(x, y)$ and their corresponding *POD* amplitudes $a_n(t)$ of disturbance pressure fields obtained for the cases with f_r = 1.11 and f_r = 2.0 at A = 0.2. Based on the values of λ_k, the first four *POD* modes contribute 99% and 78% to the disturbance pressure fields of f_r = 1.11 and f_r = 2.0 cases, respectively. For f_r = 1.11 case, the values of frequency-ratio observed for a_1 & a_2 and a_3 & a_4 are f_r = 1.11 and $2f_r$, respectively. The first two *POD* modes of f_r = 1.11 case propagate almost in the vertical direction and the next two *POD* modes propagate along horizontal directions. Hence, the first two *POD* modes contribute to lift dipole and the drag dipole is contributed by next two *POD* modes. In f_r = 2.0 case, the frequencies of a_1 & a_2 and a_3 & a_4 are identified as f_s = 1.11 and 0.0326, respectively. In case of f_r = 2.0, the first two *POD* modes contribute to lift dipole whereas the next two *POD* modes corresponds to disturbance pressure fields with modulation frequency.

4. SUMMARY AND CONCLUSIONS

In the present study, numerical simulations have been performed to characterize the sound fields generated during flow over a circular cylinder subjected to rotary oscillations using direct simulations. Flow and sound field characteristics are resolved sufficiently in the range $r \leq 100$. Fluctuations in lift and drag forces are related to the generated sound field intensities. Radiated sound fields obey theoretical decay rate in the far-field (as shown in Fig. 7 (a)). In the synchronous region, the generated sound fields are dictated by forcing frequency-ratio, whereas in the non-synchronous region, they are governed by both natural shedding frequency of stationary cylinder as well as forcing frequency of oscillation. Modulation phenomenon has been observed for the aerodynamic forces (lift and drag fluctuations) and disturbance pressure fields obtained in the non-synchronous region. The generated sound fields exhibit dipolar nature dominated by lift dipole for all values of f_r considered in the present study. The generated sound field intensity is found maximum at f_r = 1.11. Further, the *POD* analysis of disturbance pressure fields has been used to identify and quantify several dominant *POD* modes and their corresponding *POD* amplitudes.

5. ACKNOWLEDGEMENTS

Some of the present cases are simulated on a computational facility provided by Dr. Sathyanarayana A., Assistant Professor, School of Mechanical Sciences, IIT Bhubaneswar. We acknowledge him for his support.

6. REFERENCES

[1] N. Curle. The influence of solid boundaries upon aerodynamic sound. *Proc. R. Soc. Lond. A*, 231:505–514, 1955.

[2] B. Etkin, G. K. Korbacher, and R. T. Keefe. Acoustic radiation from a stationary cylinder in a finite stream (aeolian tones). *J. Acoust. Soc. Am.*, 29:30–36, 1957.

[3] J. H. Gerrard. Measurements of the sound from circular cylinders in an air stream. *Proc. Phys. Soc. Lond. B*, 68:453–461, 1955.

[4] O. M. Phillips. The intensity of aeolian tones. *J. Fluid Mech.*, 1:607–624, 1956.

[5] O. Inoue and N. Hatakeyama. Sound generation by a two-dimensional circular cylinder in a uniform flow. *J. Fluid Mech.*, 471:285–314, 2002.

[6] O. Inoue and Y. Suzuki. Beat of sound generated by flow past three side-by-side square cylinders. *Phys. Fluids*, 19(4):048102, 2007.

[7] Y. Liow, B. Tan, M. Thompson, and K. Hourigan. Sound generated in laminar flow past a two-dimensional rectangular cylinder. *J. Sound Vib.*, 295(1-2):407–427, 2006.

[8] F. Margnat. Hybrid prediction of the aerodynamic noise radiated by a rectangular cylinder at incidence. *Computers & Fluids*, 109:13–26, 2015.

[9] O. Inoue. Effect of initial condition on the sound generation by flow past a rotary-oscillating circular cylinder. *Phys. Fluids*, 18(11), 2006.

[10] Y. Hattori and R. Komatsu. Mechanism of aeroacoustic sound generation and reduction in a flow past oscillating and fixed cylinders. *J. Fluid Mech.*, 832:241–268, 2017.

[11] Naveen Ganta, Bikash Mahato, and Yogesh G Bhumkar. Analysis of sound generation by flow past a circular cylinder performing rotary oscillations using direct simulation approach. *Physics of Fluids*, 31(2):026104, 2019.

[12] P. Holmes. *Turbulence, Coherent Structures, Dynamical Systems and Symmetry*. Cambridge Univ. Press, 2012.

[13] T. K. Sengupta, V. Vijay, and N. Singh. Universal instability modes in internal and external flows. *Computers & Fluids*, 40(1):221–235, 2011.

[14] K. A. Hoffman and S. T. Chiang. Computational fluid dynamics volume i-iii. *Engineering Education System*, 2000.

[15] Bikash Mahato, Naveen Ganta, and Yogesh G Bhumkar. Direct simulation of sound generation by a two-dimensional flow past a wedge. *Physics of Fluids*, 30(9):096101, 2018.

[16] Bikash Mahato, Ganta Naveen, and Yogesh G Bhumkar. Computation of aeroacoustics and fluid flow problems using a novel dispersion relation preserving scheme. *Journal of Theoretical and Computational Acoustics*, page 1850063, 2019.

[17] J. Pradhan, S. Jindal, B. Mahato, and Y. G. Bhumkar. Joint optimization of the spatial and the temporal discretization scheme for accurate computation of acoustic problems. *Commun. Comput. Phys.*, 24(2):408–434, 2018.

[18] B Thiria, S Goujon-Durand, and JE Wesfreid. The wake of a cylinder performing rotary oscillations. *Journal of Fluid Mechanics*, 560:123–147, 2006.

[19] Tapan K Sengupta, Neelu Singh, and VK Suman. Dynamical system approach to instability of flow past a circular cylinder. *J. Fluid Mech.*, 656:82–115, 2010.

[20] L. Sirovich. Turbulence and the dynamics of coherent structures, part I-III. *Q. Appl. Maths*, 45, 1987.